TOPICAL REVIEW — Iron-based high temperature superconductors

Exploring FeSe-based superconductors by liquid ammonia method*

Ying Tian-Ping(应天平), Wang Gang(王 刚), Jin Shi-Feng(金士锋),
Shen Shi-Jie(申士杰), Zhang Han(张 韩), Zhou Ting-Ting(周婷婷),
Lai Xiao-Fang(赖晓芳), Wang Wan-Yan(王皖燕), and Chen Xiao-Long(陈小龙)†

Research & Development Center for Functional Crystals, Beijing National Laboratory for Condensed Matter Physics, Institute of Physics, Chinese Academy of Sciences, Beijing 100190, *China*

(Received 8 June 2013)

Our recent progress on the preparation of a series of new FeSe-based superconductors and the clarification of SC phases in potassium-intercalated iron selenides are reviewed here. By the liquid ammonia method, metals Li, Na, Ca, Sr, Ba, Eu, and Yb are intercalated in between FeSe layers and form superconductors with transition temperatures of 30 K∼46 K, which cannot be obtained by high-temperature routes. In the potassium-intercalated iron selenides, we demonstrate that at least two SC phases exist, $K_xFe_2Se_2(NH_3)_y$ ($x \approx 0.3$ and 0.6), determined mainly by the concentration of potassium. NH_3 has little, if any, effect on superconductivity, but plays an important role in stabilizing the structures. All these results provide a new starting point for studying the intrinsic properties of this family of superconductors, especially for their particular electronic structures.

Keywords: superconductivity, iron-based superconductor, liquid ammonia, critical temperature

PACS: 74.70.Xa, 74.25.–q, 74.62.Bf, 74.25.Dw **DOI:** 10.1088/1674-1056/22/8/087412

1. Introduction

Significant interest has been stimulated in the study of metal-intercalated iron selenides since the discovery of superconductivity at about 30 K in $K_{0.8}Fe_2Se_2$[1] and later in $Cs_{0.8}(FeSe_{0.98})_2$,[2] $Rb_xFe_ySe_2$,[3] $Tl_{0.58}Rb_{0.42}Fe_{1.72}Se_2$,[4] and $(Tl,K)Fe_xSe_2$.[5] These metal-intercalated FeSe-based superconductors exhibit several unique structural and physical characteristics compared to other Fe-based superconductors.[6,7] For example, the iron vacancies order to form supercells above 500 K, while the iron sites in other Fe-based superconductors are fully filled. Moreover, neutron diffraction reveals a blocked antiferromagnetism with pretty high ordering temperature and large magnetic moment up to 3.3 μ_B/Fe at 10 K.[8–14] Most surprisingly, electron Fermi surfaces are observed only around M points of the Brillouin zone while no hole-like Fermi surfaces are found around Γ points.[15–18] These characteristics imply that the dominant mechanism of superconductivity in these materials may be different and lead to new perspectives on understanding the Fe-based superconductors.

Considerable progress made in the study of $A_xFe_{2-y}Se_2$ (A = K, Cs, Rb, etc.) has confirmed that there are phase separations in this family of superconductors. The studies by transmission electron microscopy,[19–21] X-ray diffraction (XRD),[22–24] Mössbauer spectroscopy,[25] nuclear magnetic resonance,[26] muon spin spectroscopy,[27] scanning tunneling microscopy,[28] infrared spectroscopy,[29] and Raman spectroscopy[30] have given strong evidence that insulating phases with $\sqrt{5} \times \sqrt{5} \times 1$ superstructure and superconducting (SC) phases coexist. The insulating phases with formula $A_2Fe_4Se_5$ (the so called 245 phase) are responsible for the observed large magnetic moments. The SC phases with low volume fractions (lower than 20%) are iron vacancy free and can be represented by the formula $A_xFe_2Se_2$.[21,24,26,28] They precipitate from $A_xFe_{2-y}Se_2$ into nanoscale stripes intergrowing with the 245 phases. The deduced alkali occupancies vary a lot from $x = 0.3$ to 1.0.[24,26,28] Apart from the commonly reported 30-K phase, a 44-K SC phase with trace fraction was also occasionally observed, further complicating the identification of SC phases.[31,32] Various attempts to obtain pure or SC-dominated samples by using traditional high-temperature routes have failed so far. Therefore, it is still a pressing and important issue to obtain high-quality SC samples to study the intrinsic properties of this family of superconductors, especially for clarifying their particular electronic structures.

Here, we mainly review our recent progress in exploring new FeSe-based superconductors and indentifying the SC phases in potassium-intercalated iron selenides by the liquid ammonia (LA) method. This method implies a unique low temperature synthetic route, in contrast to the high-temperature routes. We synthesized a series of new superconductors with T_c = 30 K∼46 K by intercalating metals Li, Na, Ba, Sr, Ca, Eu, and Yb in between FeSe-layers.[33–35] We then identified that there are at least two SC phases in

*Project supported by the National Natural Science Foundation of China (Grant Nos. 90922037, 51072226, and 51202286), the Chinese Academy of Sciences, the International Center for Diffraction Data (ICDD), and the Beijing Nova Program, China (Grant No. 2011096).

†Corresponding author. E-mail: chenx29@iphy.ac.cn

© 2013 Chinese Physical Society and IOP Publishing Ltd

the potassium-intercalated iron selenides, differing mainly in potassium concentration.[36] The effect of NH_3 on structure and superconductivity is studied. A plausible structural model is proposed.

2. LA method

NH_3 is a colorless, irritant gas and can be maintained at liquid form at -77.7 °C to -33.3 °C at ambient pressure or at elevated temperatures under high pressure. LA is a well known nonaqueous solvent. Its most remarkable property is the ability to dissolve alkalis (Li, Na, K, Rb, Cs), alkaline earths (Ca, Sr, Ba), and even some rare earths (Eu, Yb) without reaction to form highly colored, electrically conductive solutions containing solvated electrons. Such homogeneous reducing agents would donate the solvated electrons from the solution to empty bands in the solid with corresponding metal cations to balance the charge. In 1959, Rudorff[37] first synthesized a variety of alkali metal intercalated sulfides in LA. Afterward, LA methods were successfully applied to intercalate metals into MoS_2, C_{60}, and MNCl (M = Zr, Hf) yielding superconductivity at 2.4 K $\sim$ 6.3 K, $\sim$ 29 K, and $\sim$ 25 K, respectively.[38–43]

In this work, we attempted to synthesize new isostructural chalgogenides with other alkali metals, alkaline earths, and some rare earths and to identify the SC phases in potassium-intercalated iron selenides. The synthesis processes were carried out in Schlenk line equipment or alternatively in autoclaves. Figure 1 shows the schematic of our Schlenk line apparatus. The finely ground β-FeSe and metals were weighed in proper ratios and loaded into a Schlenk tube, which was then connected to Schlenk line for evacuation. High purity NH_3 (99.999%) gas was then introduced into the chilled tube isolated from the vacuum line and condensed into liquid through path 1. During the process, stirring or shaking is needed to facilitate the reaction and to improve the homogeneity of the products. Finally, the cooling bath was removed and the samples were obtained by evaporating the solvent LA via path 2. For safety, a safe valve, which releases gas when the pressure exceeds 1 atm (1 atm = 1.01325×10^5 Pa), is designed to reduce the risk of explosion. As for the autoclave, all the reactants, together with LA, were sealed and kept at room temperature, where NH_3 maintains liquid form under high pressure. After the reaction, the autoclaves were opened in a glove box and the samples were rinsed by using fresh LA.

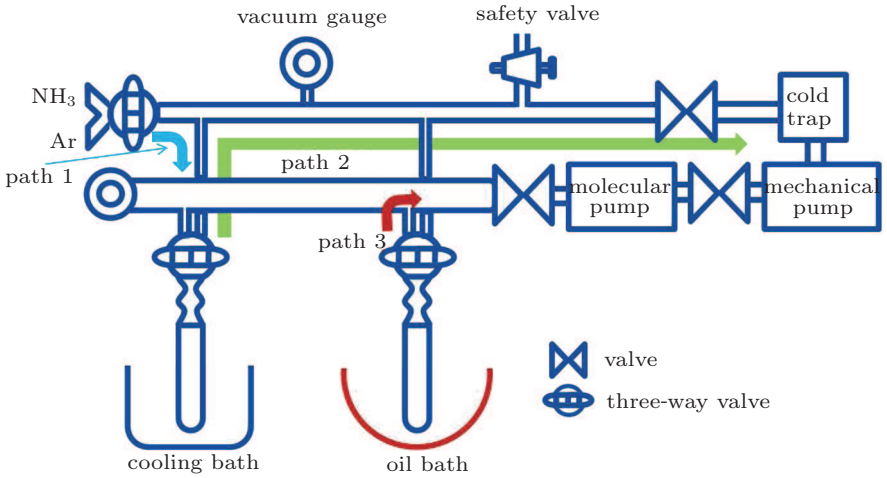


Fig. 1. Schematic of the Schlenk line equipment. Gaseous NH_3 is condensed through path 1 and evacuated through path 2. The co-intercalated NH_3 could be extracted through path 3.

3. A series of new superconductors $A_xFe_2Se_2$ (A = Li, Na, Ba, Sr, Ca, Eu, and Yb)

New isostructural chalcogenides with smaller-sized alkali metals and alkaline earths have been pursued using high-temperature routes ever since the discovery of superconductivity in $K_{0.8}Fe_2Se_2$, but all have failed. Here, we report that metals Li, Na, Ba, Sr, Ca, Eu, and Yb can be successfully intercalated in between FeSe layers by the LA method, forming a series of superconductors with $T_c = 30$ K $\sim$ 46 K. Note that 46 K is the highest value of T_c reported so far for FeSe-layer compounds under ambient pressure.

3.1. Crystallographic structures

Figure 2 shows the powder X-ray diffraction (PXRD) patterns of nominal $A_xFe_2Se_2(NH_3)_y$. Among them, $LiFe_2Se_2(NH_3)_y$, $NaFe_2Se_2(NH_3)_y$, $K_{0.6}Fe_2Se_2(NH_3)_y$, $Sr_{0.3}Fe_2Se_2(NH_3)_y$, $Ba_{0.3}Fe_2Se_2(NH_3)_y$, and $Eu_{0.3}Fe_2Se_2(NH_3)_y$ are indexed on one crystallographic unit cell. In contrast, indexing the patterns for $Ca_{0.5}Fe_2Se_2(NH_3)_y$ and $Yb_{0.8}Fe_2Se_2(NH_3)_y$ yields two unit cells. Their respective lattice constants are summarized in Table 1. All constants a are comparable with those of $K_{0.8}Fe_{1.7}Se_2$ synthesized by the high-temperature routes, while c is enlarged, suggesting that between the FeSe layers other atom groups exist, for instance, NH_3.

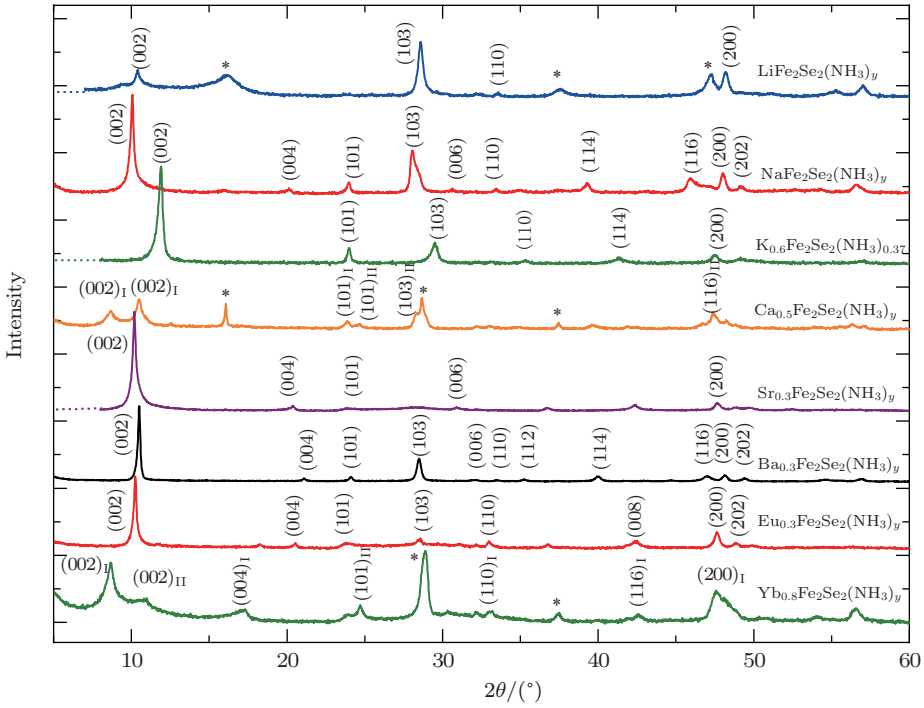


Fig. 2. PXRD patterns for nominal $LiFe_2Se_2(NH_3)_y$, $NaFe_2Se_2(NH_3)_y$, $K_{0.6}Fe_2Se_2(NH_3)_{0.37}$, $Ca_{0.5}Fe_2Se_2(NH_3)_y$, $Sr_{0.3}Fe_2Se_2(NH_3)_y$, $Ba_{0.3}Fe_2Se_2(NH_3)_y$, $Eu_{0.3}Fe_2Se_2(NH_3)_y$, and $Yb_{0.8}Fe_2Se_2(NH_3)_y$ measured at 297 K, Cu Kα radiation. Peaks marked by '*' are diffraction peaks related to residual β-FeSe.[33]

Table 1. Indexing results of $A_xFe_2Se_2(NH_3)_y$ (A = Li, Na, K, Ca, Sr, Ba, Eu, and Yb).

Sample	Unit cell	a/Å (1 Å = 10^{-10} m)	c/Å	T_c^{onset}/K	Apparatus
$LiFe_2Se_2(NH_3)_y$		3.775(5)	17.04(3)	44	autoclave
		3.8249(2)	16.5266(9)		Schlenk line[34]
$NaFe_2Se_2(NH_3)_y$		3.7846(4)	17.432(1)	46	autoclave
$K_{0.6}Fe_2Se_2(NH_3)_{0.37}$		3.822(1)	14.84(1)	30	Schlenk line
$Ca_{0.5}Fe_2Se_2(NH_3)_y$	1	3.79(1)	20.54(4)	40	autoclave
	2	3.819(3)	16.75(3)		
$Sr_{0.3}Fe_2Se_2(NH_3)_y$		3.806(2)	17.26(5)	38	Schlenk line
$Ba_{0.3}Fe_2Se_2(NH_3)_y$		3.7781(2)	16.8427(8)	39	autoclave
$Eu_{0.3}Fe_2Se_2(NH_3)_y$		3.816(1)	17.24(1)	38	Schlenk line
$Yb_{0.8}Fe_2Se_2(NH_3)_y$	1	3.831(4)	20.35(4)	43	autoclave
	2	3.79(1)	16.26 (2)		

By a similar method, Burrard-Lucas *et al.*[34] claimed that Li cations, amide anions, and ammonia molecules are intercalated simultaneously in between FeSe layers. Using neutron powder diffraction, they showed that amide anions and NH_3 molecules occupy the 8-coordinate sites in $Li_x(NH_2)_y(NH_3)_{1-y}Fe_2Se_2$ ($x \sim 0.6$; $y \sim 0.2$) and are coordinated by Li ions. Scheidt *et al.*[35] later ruled out the existence of lithium amide and attributed the superconductivity to the presence of the $Li_x(NH_3)_y$ units.

3.2. Physical properties

Figure 3 shows the M–T curves for nominal $NaFe_2Se_2(NH_3)_y$. Zero-field-cooling (ZFC) and field-cooling (FC) curves above the onset transition temperature are quite flat and nearly temperature independent. The curves sharply drop in both ZFC and FC, exhibiting a SC transition starts at

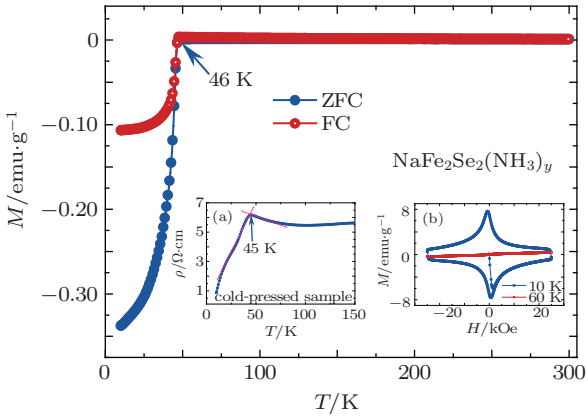


Fig. 3. The magnetization and electrical resistance of nominal $NaFe_2Se_2(NH_3)_y$. The left inset (a) shows the temperature dependence of the electrical resistance (R–T) of cold-pressed $NaFe_2Se_2(NH_3)_y$ powder. The right inset (b) shows its magnetic hysteresises (M–H) measured at 10 K and 60 K in the range -25 kOe$< H <$ 25 kOe (1 Oe = 79.5775 A/m), respectively, .[33]

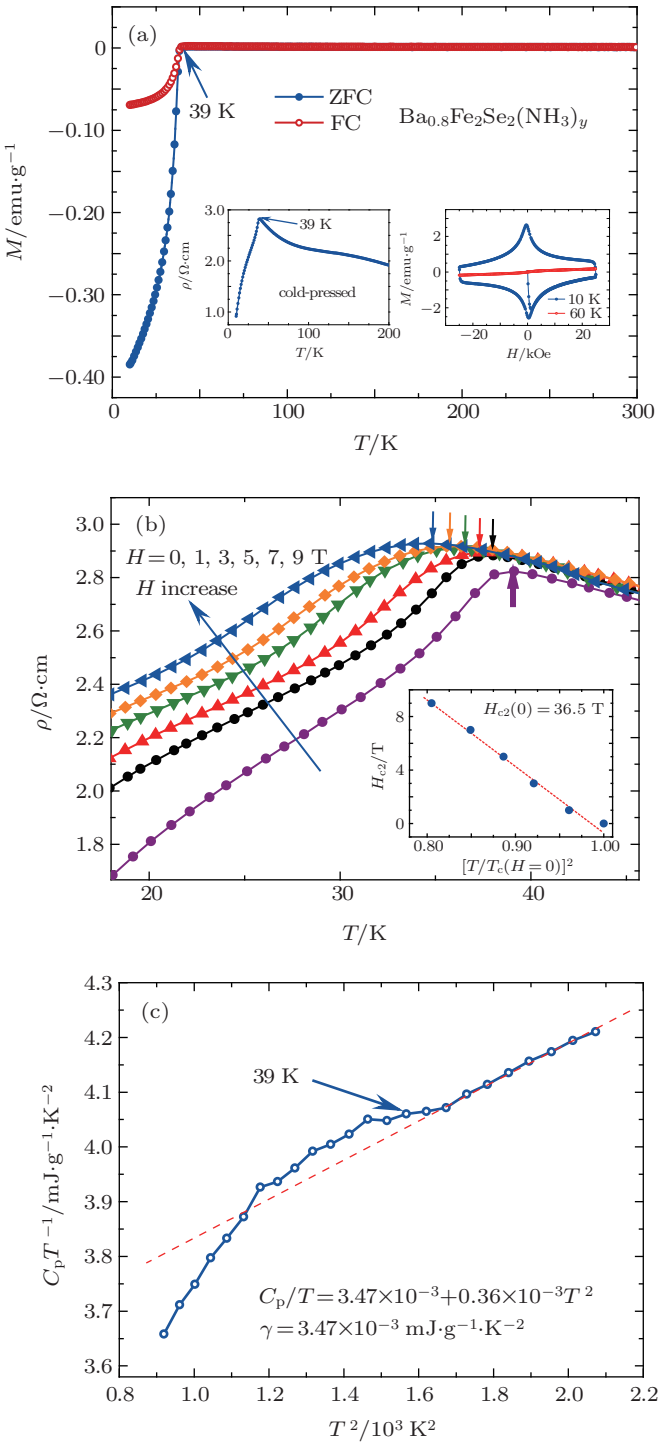


Fig. 4. Magnetization, electrical resistance, upper critical field (H_{c2}), and heat capacity of nominal $Ba_{0.8}Fe_2Se_2$. (a) The magnetization of nominal $Ba_{0.8}Fe_2Se_2(NH_3)_y$ as a function of temperature. The insets are R–T and M–H curves for $Ba_{0.8}Fe_2Se_2(NH_3)_y$. (b) The low-temperature electrical resistance for cold-pressed $Ba_{0.8}Fe_2Se_2(NH_3)_y$ powder in magnetic fields H = 0, 1 T, 3 T, 5 T, 7 T, and 9 T, respectively. The inset shows the temperature dependence of the onset T_c. The H_{c2} is estimated to be about 36.5 T. (c) Low-temperature heat capacity of cold-pressed $Ba_{0.8}Fe_2Se_2(NH_3)_y$ powder. The red dotted line is the curve fitting of phonon contribution to the heat capacity.[33]

about 46 K, comparable to the 48.7 K observed under high pressure.[44] To further confirm the SC transition, we measured its M–H curves and ρ–T curve (see inset of Fig. 3). The M–H curve at 10 K exhibits typical features of type-II superconductors. For the cold-pressed sample, though not reaching zero resistance, a sharp transition in electrical resistance at 45 K is observed.

Very similar to $NaFe_2Se_2(NH_3)_y$, $Ba_{0.8}Fe_2Se_2(NH_3)_y$ shows a SC transition at 39 K (see Fig. 4(a)), which is verified by a recent report of barium intercalated iron selenides.[45] The superconductive shielding fraction is estimated to be about 62% at 10 K. The M–H curves and ρ–T curve of $Ba_{0.8}Fe_2Se_2(NH_3)_y$, shown in the inset of Fig. 4(a), confirm its SC transition and the type-II superconductor. Its lower critical field (H_{c1}) is around 0.15 T and the upper critical field (H_{c2}) is estimated to be about 36.5 T (see Fig. 4(b)). Figure 4(c) shows the specific heat of cold-pressed $Ba_{0.8}Fe_2Se_2(NH_3)_y$. The electronic coefficient of heat capacity γ is determined to be 3.47×10^{-3} mJ·g^{-1}·K^{-2} according to the zero-temperature intercept in the normal state. At lower temperatures, a clear deviation from the linear change at 39 K is observed though without apparent peak, again confirming the nature of bulk SC in $Ba_{0.8}Fe_2Se_2(NH_3)_y$.

Moreover, $BA_xFe_2Se_2(NH_3)_y$ samples are relatively stable compared with metastable $NaFe_2Se_2(NH_3)_y$, which may gradually degrade even in a glove box. After samples are exposed to air for one day or have contact with moist air, the diffraction peaks of $Ba_{0.3}Fe_2Se_2(NH_3)_y$ show no apparent change (see Fig. 5) and its T_c remains the same. The M–T and M–H curves for other samples are shown in Fig. 6. They are all superconductors and their respective T_cs are marked with arrows. The transition temperature at 44 K in lithium doped iron selenides was later confirmed by Burrard-Lucas *et al.*[34] and Scheidt *et al.*[35]

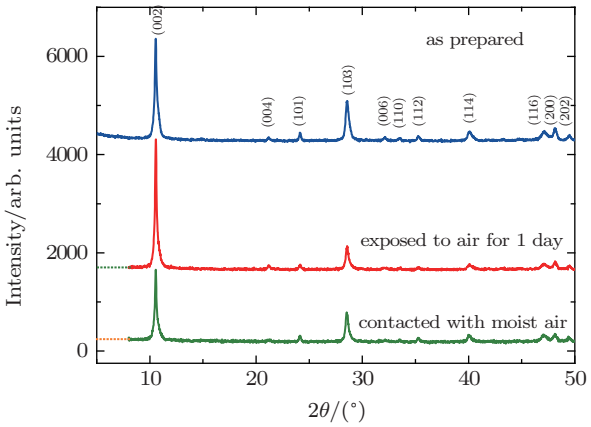


Fig. 5. The PXRD patterns of nominal $Ba_{0.3}Fe_2Se_2(NH_3)_y$ as-prepared, exposed to air for one day, and contacted by moist air, respectively.

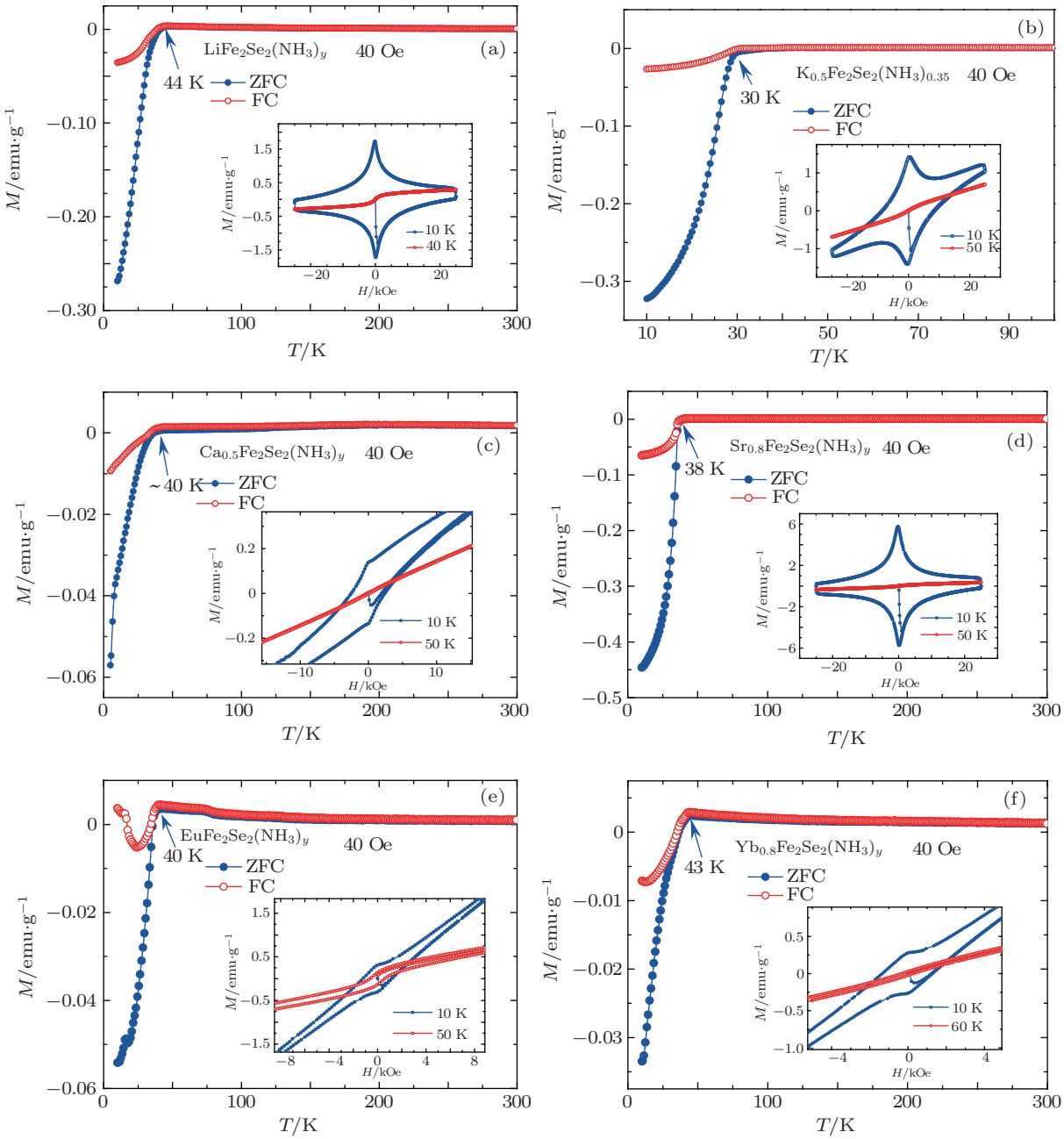


Fig. 6. The magnetization of nominal (a) $LiFe_2Se_2(NH_3)_y$,(b) $K_{0.5}Fe_2Se_2(NH_3)_{0.35}$, (c) $Ca_{0.5}Fe_2Se_2(NH_3)_y$, (d) $Sr_{0.8}Fe_2Se_2(NH_3)_y$, (e) $EuFe_2Se_2(NH_3)_y$, (f) $Yb_{0.8}Fe_2Se_2(NH_3)_y$. The insets show their respective magnetic hysteresises.[33]

4. SC phases in potassium-intercalated iron selenides

The compositions and structures for SC phases in $A_xFe_{2-y}Se_2$ ($A = K, Cs, Rb$, etc.), even though intensively investigated, still remain a mystery. The finding that SC phases have integrated FeSe layers[21,24,26,28] and the existence of a 44-K SC phase[30,31] imply that intercalated metal content may play a crucial role in inducing superconductivity. However, fine-tuning the concentrations of metals intercalated in between FeSe layers is not allowed by the high-temperature routes. The successful syntheses of $A_xFe_2Se_2(NH_3)_y$ demonstrate that LA method is an appropriate route to tune the concentrations of intercalated metals at low temperature. Moreover, low temperature is most helpful in preventing phase separation. Here, we report that in the potassium-intercalated iron selenides at least two SC phases exist, differing mainly in potassium concentration. One is close to $K_{0.3}Fe_2Se_2(NH_3)_{0.47}$ with $T_c = 44$ K, and the other is close to $K_{0.6}Fe_2Se_2(NH_3)_{0.37}$ with $T_c = 30$ K. Both are iron vacancy free and have no antiferromagnetic ordering.

4.1. Identification of SC phases

A variety of compounds $K_xFe_2Se_2(NH_3)_y$ with x ranging from 0.1 to 1 (their composition, T_c, and superconductive volume fraction are summarized in Table 2) were

synthesized by the LA method. The PXRD patterns for $K_xFe_2Se_2(NH_3)_y$ with $x = 0.25$, 0.4, and 0.65 are picked up to represent the FeSe-residual, mixed, and potassium over-doped regions, respectively (see Fig. 7(a)). Standard reference material Si was added to correct the diffraction peak positions. All the patterns could be indexed as a body-centered tetragonal cell with similar lattice constants a but distinct values of c with discrepancies up to about 1 Å due to varying potassium concentration. From the magnified pattern for the (002) peak in Fig. 7(b), we can clearly see that the peak shifts are not continuous with the potassium content. Instead, only two distinguished peaks at 11.36° and 11.89° are observed. $K_{0.25}Fe_2Se_2(NH_3)_{0.47}$ exhibits one (002) peak at $2\theta = 11.36°$, and $K_{0.65}Fe_2Se_2(NH_3)_{0.35}$ at $2\theta = 11.89°$, indicating these samples mainly consist of only one phase. However, $K_{0.4}Fe_2Se_2(NH_3)_{0.5}$ has two (002) peaks, containing both phases.

Table 2. Composition, T_c, and superconductive volume fraction for $K_xFe_2Se_2(NH_3)_y$.

Sample	Nominal composition	Composition by ICP-AES and Micro-Kjeldahl method	T_c/K	Superconductive volume fraction/10 K
1	$K_{0.1}Fe_2Se_2$+NH_3	–	44	10%
2	$K_{0.2}Fe_2Se_2$+NH_3	$K_{0.2}Fe_{2.03}Se_2(NH_3)_{0.45}$	44	21%
3	$K_{0.25}Fe_2Se_2$+NH_3	$K_{0.24}Fe_{1.98}Se_2(NH_3)_{0.49}$	44	40%
4	$K_{0.27}Fe_2Se_2$+NH_3	$K_{0.26}Fe_{2.01}Se_2(NH_3)_{0.45}$	44	44%
5	$K_{0.3}Fe_2Se_2$+NH_3	$K_{0.28}Fe_{1.97}Se_2(NH_3)_{0.47}$	44	45%
6	$K_{0.35}$ Fe_2Se_2+NH_3	$K_{0.33}$ $Fe_{1.96}Se_2(NH_3)_{0.4}$	43.5 & 36 & 30	41%
7	$K_{0.4}$ Fe_2Se_2+NH_3	$K_{0.4}Fe_2Se_2(NH_3)_{0.5}$	43.5 & 36 & 30	37%
8	$K_{0.45}$ Fe_2Se_2+NH_3	$K_{0.44}Fe_{1.98}Se_2(NH_3)_{0.4}$	43.5 & 36 & 30	55%
9	$K_{0.5}Fe_2Se_2$+NH_3	$K_{0.48}$ $Fe_{2.02}Se_2(NH_3)_{0.35}$	43.5 & 36 & 30	63%
10	$K_{0.6}$ Fe_2Se_2+NH_3	$K_{0.6}$ $Fe_2Se_2(NH_3)_{0.37}$	30	52%
11	$K_{0.65}Fe_2Se_2$+NH_3	$K_{0.62}Fe_2Se_2(NH_3)_{0.35}$	30	48%
12	$K_{0.7}Fe_2Se_2$+NH_3	$K_{0.57}Fe_{2.02}Se_2(NH_3)_{0.34}$	30	41%
13	$K_{0.8}Fe_2Se_2$+NH_3	$K_{0.68}Fe_2Se_2(NH_3)_{0.3}$	30	48%
14	KFe_2Se_2+NH_3	–	30	30%

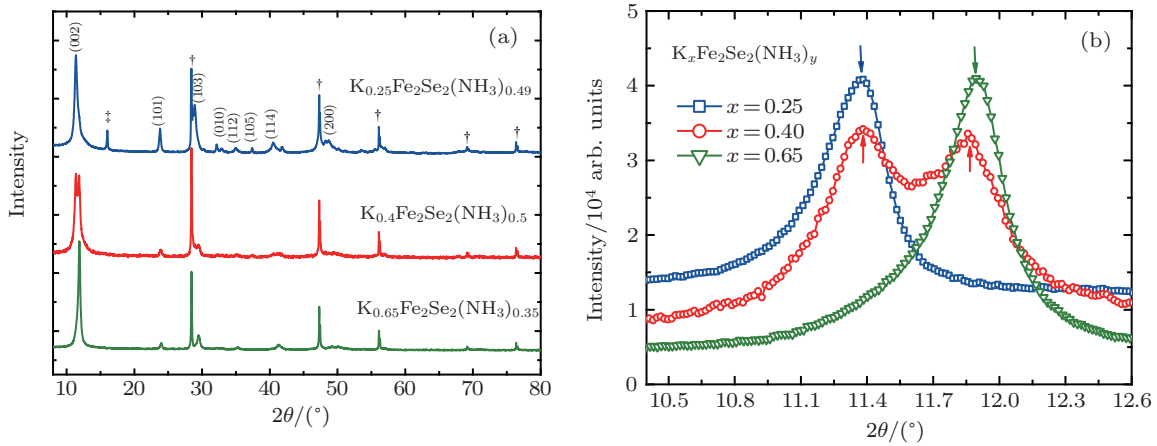


Fig. 7. (a) PXRD patterns for nominal $K_xFe_2Se_2(NH_3)_y$ ($x = 0.25$, 0.4, and 0.65, respectively) measured at 297 K, Cu Kα radiation. The patterns were referenced against Si powder, denoted with '†'. For $x = 0.25$, residual β-FeSe denoted with '‡' is observed. With increasing potassium content, the lattice with larger cell constant c weakens and another lattice with smaller c develops. The coexistence of these two phases is clearly seen at $x = 0.4$. For $x = 0.4$ and 0.65, no peaks corresponding to β-FeSe are observed. (b) The enlargement of (002) peaks. The peaks are marked with arrows.[36]

The M–T curves under FC for $K_{0.25}Fe_2Se_2(NH_3)_{0.49}$, $K_{0.4}Fe_2Se_2(NH_3)_{0.5}$, and $K_{0.65}Fe_2Se_2(NH_3)_{0.35}$ are presented in Fig. 8. Only one transition temperature is observed for $K_{0.25}Fe_2Se_2(NH_3)_{0.49}$ and $K_{0.65}Fe_2Se_2(NH_3)_{0.35}$ at 44 K and 30 K, respectively, which can be regarded 44 K and 30 K phase-dominated. In contrast with them, there is an inflection point at 30 K apart from the onset T_c at 44 K for $K_{0.4}Fe_2Se_2(NH_3)_{0.5}$, implying that two SC phases coexist.

All data for transition temperatures T_c and lattice constants c are summarized in Figs. 9(a) and 9(b). With $x < 0.3$, samples exhibit onset T_c at 44 K and lattice constants c of 15.56(1) Å. While with $x > 0.6$, all samples exhibit onset T_c at 30 K and c of 14.84(1) Å. These two phases are isostructural to each other, except for the former phase's lattice a shrinking a little and c expanding in comparison with those of the latter. Between the two critical points, namely $0.3 < x < 0.6$, these

two SC phases coexist. This discrete behavior of T_c versus

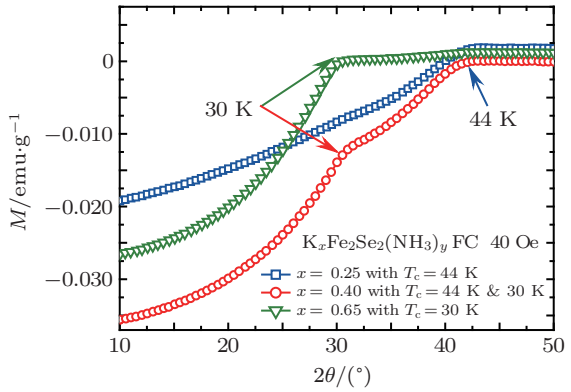


Fig. 8. FC M–T curves of samples with different nominal potassium contents. When $x = 0.25$ and 0.4, onset T_c at 44 K is observed. An inflexion point at 30 K can also be clearly seen for $K_{0.4}Fe_2Se_2(NH_3)_{0.5}$. For $x = 0.65$, T_c shifts to 30 K.[36]

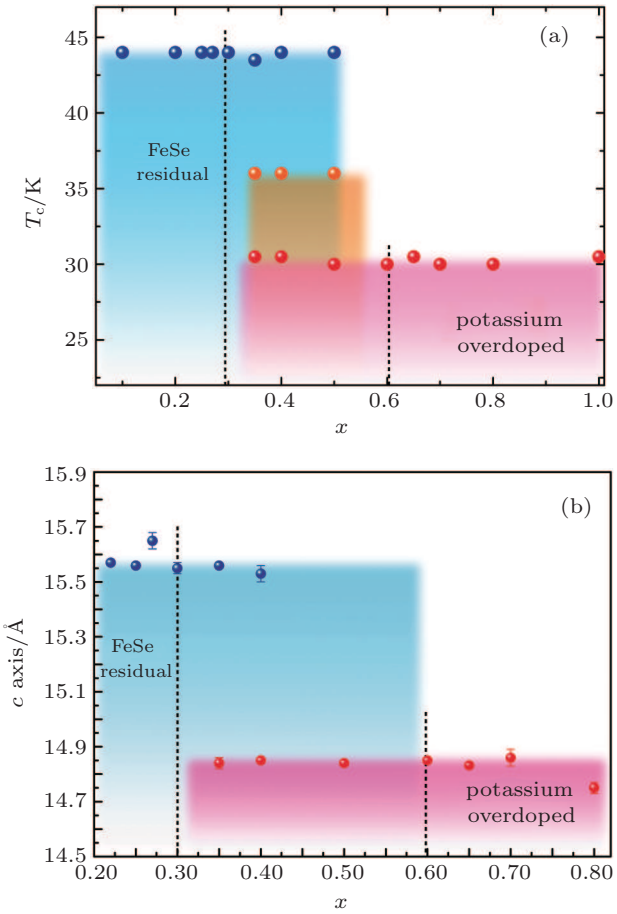


Fig. 9. (a) T_cs of $K_xFe_2Se_2(NH_3)_y$ as a function of nominal potassium contents x. They show abrupt changes against potassium content rather than dome-like ones. With x lower than 0.3 or higher than 0.6, there is residual β-FeSe or potassium. Between these two critical points, at least two T_cs exist. (b) Lattice constants c of $K_xFe_2Se_2(NH_3)_y$ versus nominal potassium content. Two distinct values of c are displayed. For x between 0.3 and 0.6, these two c coexist.[36]

potassium doping in $K_xFe_2Se_2(NH_3)_y$ makes these materials stand out among the known superconductors, as their structures are stable only at particular potassium doping levels, and hence the variation of T_c with doping is not dome-like.

The decrease of T_c from 44 K to 30 K with the increase of potassium doping from 0.3 to 0.6 implies that $K_{0.6}Fe_2Se_2(NH_3)_{0.37}$ is electron overdoped. Even for $K_{0.3}Fe_2Se_2(NH_3)_{0.47}$ yielding 0.15 electron per iron, it is still higher than the doping level of single-layer FeSe films with a much enhanced T_c (about 0.1 electron per iron),[46,47] implying that $K_{0.3}Fe_2Se_2(NH_3)_{0.47}$ may be still overdoped.

4.2. Effect of NH_3

NH_3 can be co-intercalated with metals into varied layered compounds, as discovered long ago. Co-intercalated NH_3 has been proven to assist in the insertion of the metal atoms by opening up the layers, minimizing the polarization of the lattice by the metal ion, and thereby, enhancing the diffusion of the metal ion. While the NH_3 can be subsequently removed by vacuum treatment or heating,[48] some of these compounds are stable only if the NH_3 is retained, such as lithium-intercalated MoS_2, WS_2, SnS_2, and β-FeSe.[34]

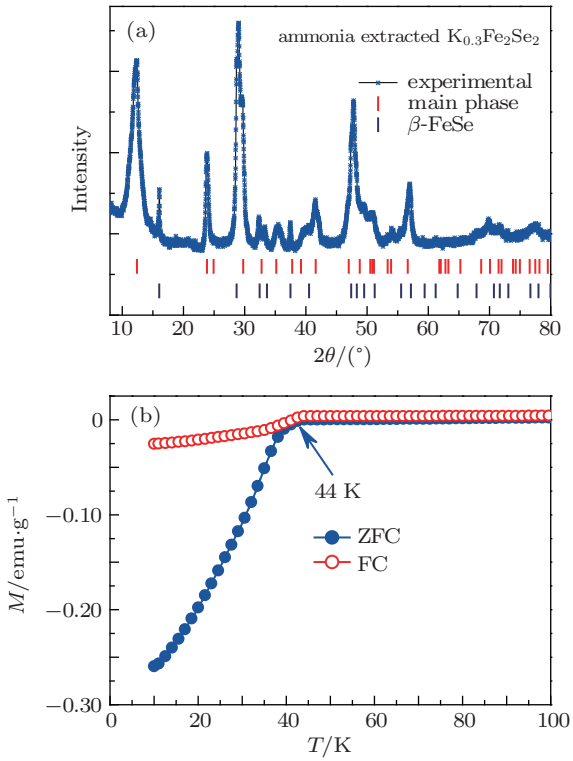


Fig. 10. (a) The PXRD pattern of nominal $K_{0.3}Fe_2Se_2$ after NH_3 extraction. The main phase can be indexed as a body-centered tetragonal cell with lattice constants $a = 3.87(1)$ Å and $c = 14.28(4)$ Å. (b) ZFC and FC curves of nominal $K_{0.3}Fe_2Se_2$ after NH_3 extraction. Transition at 44 K can be clearly seen.[36]

The existence of NH_3 and its amount in metal-intercalated iron selenides can be determined directly by a chemical titration method or deduced from neutron powder diffraction. But its influence on the superconductivity is not clear yet. Burrard-Lucas *et al.* suggest that the enhancement of the SC transition temperature of lithium-intercalated iron selenide results from the combined effect of the increase in the separation of the FeSe layers and electron doping.[34]

We extracted NH_3 from the samples and studied its influence on structure and superconductivity. The as-prepared samples were loaded in the Schlenk tube, which was placed in an oil bath and slowly heated to 200 °C to avoid the collapse of the lattice, and evacuated through path 3 for several hours (see Fig. 1). The PXRD pattern (see Fig. 10(a)) shows that the phase remains while the lattice constants change after the NH_3 extraction. Lattice constant a expands from 3.843(1) Å to 3.87(1) Å and c shrinks a lot from 15.56(1) Å to 14.28(4) Å, which is very close to that of the SC phase obtained by high-temperature routes.[21,24,28] The prominent change of c shows that NH_3 is successfully extracted from the sample. The temperature-dependant magnetization in Fig. 10(b) shows the onset T_c is still close to 44 K. These results demonstrate that NH_3 has little, if any, effect on T_c, T_c is almost the same even NH_3 is replaced by pyridine for $Li_xFe_2Se_2(C_5H_5N)_y$, which further confirms that the neutral spacers, such as NH_3 and pyridine, do not influence the superconductivity.[49]

4.3. A tentative structure of SC phases

The inserted NH_3 is very likely to form hydrogen bonds.[34] A very tentative structure model is proposed in Fig. 11. NH_3 is positioned through forming hydrogen bonds with Se. The occupancy of potassium that is bonded with nitrogen is not energetically favorable, as its concentration is roughly in an inverse proportion with NH_3 determined by chemical analyses (see Table 2). The concentration of vacancies is also low, since the sum of potassium content x and the NH_3 content y is close to $0.65 \sim 0.98$. Potassium tends to occupy the body-centered site and drive NH_3 away from the unit cell when potassium contents increase.

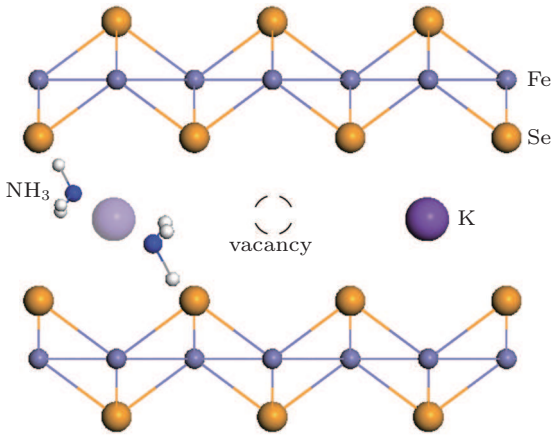


Fig. 11. A tentative structure model showing the occupancy of potassium, vacancies, and NH_3 in between the FeSe layers viewed from [100] direction.

5. Summary and perspective

The LA method provides an effective way to intercalate all the alkalis, most alkaline earths (except Be and Mg) and some rare earths (Eu and Yb) into layered compound. In this paper, our recent progress concerning the syntheses of a series of new FeSe-based superconductors and the clarification of SC phases in potassium-intercalated iron selenides via the LA method are reviewed. It is the metal content or electron concentration that determines the superconductivity of metal-intercalated iron selenides. The discrete T_c, which makes metal-intercalated iron selenides distinct from any other superconductors, is due to their structures being stable only at particular doping levels. From the point of view of optimal doping, the electron number per iron atom is still a little bit high in the obtained metal-intercalated iron selenides. Fine-tuning the concentrations of metals intercalated in between FeSe layers may lead to higher transition temperatures in this family of superconductors.

References

[1] Guo J G, Jin S F, Wang G, Wang S C, Zhu K X, Zhou T T, He M and Chen X L 2010 *Phys. Rev. B* **82** 180520

[2] Krzton-Maziopa A, Shermadini Z, Pomjakushina E, Pomjakushin V, Bendele M, Amato A, Khasanov R, Luetkens H and Conder K 2011 *J. Phys.: Condens. Matter* **23** 052203

[3] Wang A F, Ying J J, Yan Y J, Liu R H, Luo X G, Li Z Y, Wang X F, Zhang M, Ye G J, Cheng P, Xiang Z J and Chen X H 2011 *Phys. Rev. B* **83** 060512

[4] Wang H D, Dong C H, Li Z J, Mao Q H, Zhu S S, Feng C M, Yuan H Q and Fang M H 2011 *Europhys. Lett.* **93** 47004

[5] Fang M H, Wang H D, Dong C H, Li Z J, Feng C M, Chen J and Yuan H Q 2011 *Europhys. Lett.* **94** 27009

[6] Wen H H 2012 *Rep. Prog. Phys.* **75** 112501

[7] Dagotto E 2013 *Rev. Mod. Phys.* **85** 849

[8] Ye F, Chi S, Bao W, Wang X F, Ying J J, Chen X H, Wang H D, Dong C H and Fang M 2011 *Phys. Rev. Lett.* **107** 137003

[9] Liu R, Luo X, Zhang M, Wang A, Ying J, Wang X, Yan Y, Xiang Z, Cheng P and Ye G 2011 *Europhys. Lett.* **94** 27008

[10] Pomjakushin V Y, Pomjakushina E V, Krzton-Maziopa A, Conder K and Shermadini Z 2011 *J. Phys.: Condens. Matter* **23** 156003

[11] Shermadini Z, Krzton-Maziopa A, Bendele M, Khasanov R, Luetkens H, Conder K, Pomjakushina E, Weyeneth S, Pomjakushin V, Bossen O and Amato A 2011 *Phys. Rev. Lett.* **106** 117602

[12] Bao W, Huang Q Z, Chen G F, Green M A, Wang D M, He J B and Qiu Y M 2011 *Chin. Phys. Lett.* **28** 086104

[13] Wang M, Wang M, Li G N, Huang Q, Li C H, Tan G T, Zhang C L, Cao H, Tian W, Zhao Y, Chen Y C, Lu X Y, Sheng B, Luo H Q, Li S L, Fang M H, Zarestky J L, Ratcliff W, Lumsden M D, Lynn J W and Dai P 2011 *Phys. Rev. B* **84** 094504

[14] Pomjakushin V Y, Krzton-Maziopa A, Pomjakushina E V, Conder K, Chernyshov D, Svitlyk V and Bosak A 2012 *J. Phys.: Condens. Matter* **24** 435701

[15] Qian T, Wang X P, Jin W C, Zhang P, Richard P, Xu G, Dai X, Fang Z, Guo J G, Chen X L and Ding H 2011 *Phys. Rev. Lett.* **106** 187001

[16] Zhang Y, Yang L X, Xu M, Ye Z R, Chen F, He C, Xu H C, Jiang J, Xie B P, Ying J J, Wang X F, Chen X H, Hu J P, Matsunami M, Kimura S and Feng D L 2011 *Nat. Mater.* **10** 273

[17] Mou D X, Liu S, Jia X W, He J F, Peng Y, Zhao L, Yu L, Liu G D, He S L, Dong X L, Zhang J, Wang H D, Dong C H, Fang M H, Wang X Y, Peng Q J, Wang Z M, Zhang S J, Yang F, Xu Z Y, Chen C T and Zhou X J 2011 *Phys. Rev. Lett.* **106** 107001

[18] Zhao L, Mou D, Liu S, Jia X, He J, Peng Y, Yu L, Liu X, Liu G, He S, Dong X, Zhang J, He J B, Wang D M, Chen G F, Guo J G, Chen X L, Wang X, Peng Q, Wang Z, Zhang S, Yang F, Xu Z, Chen C and Zhou X J 2011 *Phys. Rev. B* **83** 140508

[19] Wang Z, Song Y J, Shi H L, Wang Z W, Chen Z, Tian H F, Chen G F, Guo J G, Yang H X and Li J Q 2011 *Phys. Rev. B* **83** 140505

[20] Chen F, Xu M, Ge Q Q, Zhang Y, Ye Z R, Yang L X, Jiang J, Xie B P, Che R C, Zhang M, Wang A F, Chen X H, Shen D W, Hu J P and Feng D L 2011 *Phys. Rev. X* **1** 021020

[21] Wang Z W, Wang Z, Song Y J, Ma C, Cai Y, Chen Z, Tian H F, Yang H X, Chen G F and Li J Q 2012 *J. Phys. Chem. C* **116** 17847

[22] Ricci A, Poccia N, Campi G, Joseph B, Arrighetti G, Barba L, Reynolds M, Burghammer M, Takeya H, Mizuguchi Y, Takano Y, Colapietro M, Saini N L and Bianconi A 2011 *Phys. Rev. B* **84** 060511

[23] Ricci A, Poccia N, Joseph B, Arrighetti G, Barba L, Plaisier J, Campi G, Mizuguchi Y, Takeya H, Takano Y, Saini N L and Bianconi A 2011 *Supercond. Sci. Technol.* **24** 082002

[24] Shoemaker D P, Chung D Y, Claus H, Francisco M C, Avci S, Llobet A and Kanatzidis M G 2012 *Phys. Rev. B* **86** 184511

[25] Ksenofontov V, Wortmann G, Medvedev S A, Tsurkan V, Deisenhofer J, Loidl A and Felser C 2011 *Phys. Rev. B* **84** 180508

[26] Texier Y, Deisenhofer J, Tsurkan V, Loidl A, Inosov D S, Friemel G and Bobroff J 2012 *Phys. Rev. Lett.* **108** 237002

[27] Shermadini Z, Krzton-Maziopa A, Bendele M, Khasanov R, Luetkens H, Conder K, Pomjakushina E, Weyeneth S, Pomjakushin V, Bossen O and Amato A 2011 *Phys. Rev. Lett.* **106** 117602

[28] Li W, Ding H, Deng P, Chang K, Song C, He K, Wang L, Ma X, Hu J P, Chen X and Xue Q K 2012 *Nat. Phys.* **8** 126

[29] Yuan R H, Dong T, Song Y J, Zheng P, Chen G F, Hu J P, Li J Q and Wang N L 2012 *Sci. Rep.* **2** 221

[30] Zhang A M, Xiao J H, Li Y S, He J B, Wang D M, Chen G F, Normand B, Zhang Q M and Xiang T 2012 *Phys. Rev. B* **85** 214508

[31] Wang D M, He J B, Xia T L and Chen G F 2011 *Phys. Rev. B* **83** 132502

[32] Zhang A M, Xia T L, Liu K, Tong W, Yang Z R and Zhang Q M 2012 *Sci. Rep.* **3** 1216

[33] Ying T P, Chen X L, Wang G, Jin S F, Zhou T T, Lai X F, Zhang H and Wang W Y 2012 *Sci. Rep.* **2** 426

[34] Burrard-Lucas M, Free D G, Sedlmaier S J, Wright J D, Cassidy S J, Hara Y, Corkett A J, Lancaster T, Baker P J, Blundell S J and Clarke S J 2013 *Nat. Mater.* **12** 15

[35] Scheidt E W, Hathwar V R, Schmitz D, Dunbar A, Scherer W, Mayr F, Tsurkan V, Deisenhofer J and Loidl A 2012 *Eur. Phys. J. B* **85** 279

[36] Ying T P, Chen X L, Wang G, Jin S F, Lai X F, Zhou T T, Zhang H, Shen S J and Wang W Y 2013 *J. Am. Chem. Soc.* **135** 2951

[37] Rudorff W 1965 *Chimia* **19** 489

[38] Somoano R B and Rembaum A 1971 *Phys. Rev. Lett.* **27** 402

[39] Somoano R B, Hadek V and Rembaum A 1973 *J. Chem. Phys.* **58** 697

[40] Subba Rao G V, Shafer M W, Kawarazaki S and Toxen A M 1974 *J. Solid State Chem.* **9** 323

[41] Buffinger D R, Ziebarth R P, Stenger V A, Recchia C and Pennington C H 1993 *J. Am. Chem. Soc.* **115** 9267

[42] Ye G J, Ying J J, Yan Y J, Luo X G, Cheng P, Xiang Z J, Wang A F and Chen X H 2012 *Phys. Rev. B* **86** 134501

[43] Zhang S, Yanaka M, Onimaru T, Takabatake T, Isikawa Y and Ymanaka S 2013 *Supercond. Sci. Technol.* **26** 045017

[44] Sun L L, Chen X J, Guo J, Gao P, Huang Q Z, Wang H, Fang M, Chen X, Chen G, Wu Q, Zhang C, Gu D, Dong X, Wang L, Yang K, Li A, Dai X, Mao H K and Zhao Z 2012 *Nature* **483** 67

[45] Shibasaki S, Ashida K, Takahei Y, Tomita K, Kumai R and Kambe T 2013 arXiv: 1306.0979

[46] Liu D F, Zhang W H, Mou D X, He J F, Ou Y B, Wang Q Y, Li Z, Wang L L, Zhao L, He S L, Peng Y Y, Liu X, Chen C Y, Xu L, Lin G D, Dong X L, Zhang J, Chen C T, Xu Z Y, Hu J P, Chen X, Ma X C, Xue Q K and Zhou X J 2012 *Nat. Commun.* **3** 931

[47] He S L, He J F, Zhang W H, Zhao L, Liu D F, Liu X, Mou D X, Ou Y B, Wang Q Y, Li Z, Wang L L, Peng Y Y, Liu Y, Chen C Y, Yu L, Liu G D, Dong X L, Zhang J, Chen C T, Xu Z Y, Chen X, Ma X C, Xue Q K and Zhou X J 2013 *Nat. Mater.* **12** 605

[48] Whittingham M S 1978 *Prog. Solid State Chem.* **12** 41

[49] Krzton-Maziopa A, Pomjakushina E V, Pomjakushin V Y, Rohr F V, Schilling A and Conder K 2012 *J. Phys.: Condens. Matter* **24** 382202